Epsilon: Jurnal Matematika Murni dan Terapan
http://ppjp.ulm.ac.id/journals/index.php/epsilon
p-ISSN: 1978-4422 | e-ISSN 2656-7660
Vol.20 No.1 (Juni 2026) Hal. 119-146

INVESTIGATION OF THE IMPACT OF ONE-WAY MOBILITY IN A MATHEMATICAL MODEL OF COVID-19 TRANSMISSION: STABILITY ANALYSIS AND NUMERICAL SIMULATIONS

Muhammad Afief Balya*, Yuni Yulida, Sila Rizqina, Hermei Lissa

Department of Mathematics, Faculty of Mathematics and Natural Sciences,
Universitas Lambung Mangkurat
Jl. Ahmad Yani Km.36, Banjarbaru, South Kalimantan, 70714, Indonesia
*email: *afief.balya@ulm.ac.id*

ABSTRACT

This study develops a COVID-19 transmission model incorporating one-way human mobility between two interconnected cities to examine the epidemiological consequences of asymmetric population movement. Unlike most existing models that assume symmetric two-way mobility, and extending the no-mobility framework of (Balya et al., 2025), the proposed model introduces unidirectional population flow by allowing individuals from only one city to engage in high-mobility activities, thereby generating directed movement that reflects realistic patterns such as commuting, migration, and unequal social interaction. The basic reproduction number $\mathcal{R}_0$ is analytically derived using the Next Generation Matrix approach, and the stability of the disease-free equilibrium is established through the Van den Driessche–Watmough method. Elasticity analysis demonstrates that mobility-related parameters substantially increase $\mathcal{R}_0$, while recovery and mortality parameters reduce it, highlighting key factors that drive transmission under directed movement. Numerical simulations across three epidemiological scenarios, defined by the relative ordering of the two cities' no-mobility reproduction numbers, show that one-way mobility raises the basic reproduction number of the coupled system to approximately 3.99, 2.10, and 1.62, respectively, and consistently elevates infection levels in both cities, even when one city is subcritical in isolation, due to both imported infections and intensified local contact rates. These results suggest that mobility-sensitive interventions, such as movement restrictions on high-mobility populations or social distancing measures in high-transmission cities are essential to prevent directed population flow from destabilizing epidemic control across interconnected regions.

Keywords: COVID-19, One-Way Mobility, Basic Reproduction Number, Elasticity Analysis, Numerical Simulations.

Received: 16 March 2026, Accepted: 16 July 2026, Published: 20 July 2026

INTRODUCTION

The Coronavirus Disease 2019 (COVID-19), caused by the Severe Acute Respiratory Syndrome Coronavirus 2 (SARS-CoV-2), has significantly affected global public health systems and mobility patterns. Since the virus spreads primarily through direct or indirect contact among individuals, human movement has become one of the major drivers of COVID-19 transmission across regions.

Various countries have implemented non-pharmaceutical interventions such as lockdowns, travel restrictions, and large-scale social distancing to suppress the spread of the disease (Flaxman et al., 2021), (Li et al., 2020). At the same time, mathematical models have been widely developed to analyze COVID-19 transmission dynamics and evaluate the effectiveness of control strategies. These models serve as valuable tools for predicting epidemic trends, measuring the impact of interventions, and supporting data-driven policymaking in public health (He et al., 2020), (Yang & Wang, 2020).

Numerous studies have incorporated human mobility into epidemic models to capture the spatial spread of infectious diseases. Recent works have demonstrated that mobility reduction is strongly associated with decreasing transmission rates, highlighting its importance in epidemic control (Badr et al., 2021), (Jia et al., 2021). More recent metapopulation and gravity-based frameworks have further quantified how the volume and direction of inter-regional movement shape COVID-19 transmission between connected regions (Iyaniwura et al., 2023). However, most existing models adopt a two-way (symmetric) mobility structure, where population movement between regions is assumed to be balanced in both directions (Pei & Shaman, 2021), (Lin et al., 2021). In reality, mobility is often unidirectional, such as in migration flows, commuter patterns, and permanent relocation, which can generate asymmetric transmission risks. Therefore, a more realistic approach is required to better understand the influence of directed population flow on the spread of COVID-19.

One-way mobility has the potential to alter epidemic dynamics in ways that differ from two-way mobility assumptions. A continuous unidirectional inflow of individuals can create a persistent source of infection in the destination region, even when local interventions are effective. Conversely, the origin region may experience different epidemiological behavior due to population outflow without return. Despite its importance, mathematical investigations focusing specifically on one-way mobility in COVID-19 models remain limited in the literature. This gap indicates the need to explore the role of directed movement to generate a more comprehensive understanding of spatial disease transmission.

A previous study examined the transmission dynamics of COVID-19 in two regions without any human mobility, where each population evolved independently based on its local parameters (Balya et al., 2025). The study showed that the persistence of the disease is determined solely by internal regional factors, reflected through the basic reproduction number. However, the assumption of zero mobility does not represent real conditions, as inter-regional interactions are common and can significantly change epidemic outcomes. Extending the model by introducing one-way mobility is therefore essential to better reflect realistic transmission patterns. By comparing these two scenarios, the influence of directed movement on epidemic behavior can be more clearly identified.

This research aims to investigate the impact of one-way human mobility on the transmission dynamics of COVID-19 by developing an extended compartmental model. The proposed model analyzes how directed movement affects the basic reproduction number, equilibrium behavior, and spatial spread of the disease. The results are expected to provide theoretical insights into mobility-sensitive public health strategies and offer a better understanding of spatial epidemic control. The novelty of this work lies in incorporating a unidirectional mobility structure and examining its epidemiological consequences through analytical and numerical approaches. Thus, this study contributes both to the development of mathematical epidemiology and to practical considerations for designing more effective mobility-based intervention policies.

PRELIMINARIES

Nonlinear System of Differential Equations

Definition 1. A first-order nonlinear system of differential equations can be written in matrix form as follows.

$$\frac{d\boldsymbol{X}}{dt} = \boldsymbol{F}(t, \boldsymbol{X}),$$

where

$$\boldsymbol{X} = \begin{bmatrix} x_1(t) \\ x_2(t) \\ \vdots \\ x_n(t) \end{bmatrix}, \text{ and } \boldsymbol{F}(t, \boldsymbol{X}) = \begin{bmatrix} f_1(t, x_1, x_2, \dots, x_n) \\ f_2(t, x_1, x_2, \dots, x_n) \\ \vdots \\ f_n(t, x_1, x_2, \dots, x_n) \end{bmatrix}. \quad (1)$$

$\boldsymbol{F}(t, \boldsymbol{X})$ is referred to as a function that is nonlinear with respect to the variables $x_1, x_2, \dots, x_n$ (Braun, 1993).

SIR Model

The SIR model by Kermack and McKendrick is a classical mathematical model used in epidemiology to describe the spread of infectious diseases. It divides the population into three compartments:

- S (Susceptible): Individuals who are susceptible to the disease but not yet infected.
- I (Infected): Individuals who are currently infected and capable of spreading the disease.
- R (Recovered): Individuals who have recovered from the disease and gained immunity or have been removed from the population due to death (Martcheva, 2015).

The SIR model is typically represented by the following system of ordinary differential equations (ODEs):

$$\frac{dS}{dt} = -\beta SI$$

$$\frac{dI}{dt} = \beta SI - rI$$
$$\frac{dR}{dt} = rI$$

where:
β : disease transmission rate; $\beta > 0$
r : disease recovery rate; $r > 0$
(Martcheva, 2015).

Equilibrium Point

Definition 2. Given the following autonomous system of ordinary differential equations:

$$\dot{\boldsymbol{x}} = \boldsymbol{f}(\boldsymbol{x}), \quad \boldsymbol{x} \in \mathbb{R}^n \tag{2}$$

The equilibrium solution of the system in equation (2) is the point $\bar{\boldsymbol{x}} \in \mathbb{R}^n$ such that

$$\boldsymbol{f}(\bar{\boldsymbol{x}}) = \boldsymbol{0},$$

where the equilibrium point, which is the solution to equation (2), does not change over time. This equilibrium point is also commonly referred to as a stationary point, rest point, or steady state (Wiggins, 2003).

Linearization of a System of Nonlinear Differential Equations

Definition 3. If $\boldsymbol{x} = \bar{\boldsymbol{x}} \in \mathbb{R}^{\boldsymbol{n}}$ is an equilibrium solution of the differential equation system (2) and f is a nonlinear function, then the linearization of the differential equation system (2) around the equilibrium point $\bar{\boldsymbol{x}}$ is as follows:

$$\boldsymbol{x}' = \boldsymbol{J}(\boldsymbol{x} - \bar{\boldsymbol{x}}), \tag{3}$$

where $\boldsymbol{x}$ is the dependent variable with n components, namely $x_1, x_2, \dots, x_n$ so that the components of $\boldsymbol{f}(\boldsymbol{x})$ consist of $f_1(\boldsymbol{x}), f_2(\boldsymbol{x}), \dots, f_n(\boldsymbol{x})$ and these components must have at least continuous second derivatives. Therefore, a constant matrix $\boldsymbol{J}$ of size $n \times n$ is also defined in equation (3), which is the matrix of the first partial derivatives of the components of $\boldsymbol{f}(\boldsymbol{x})$ with respect to the components of $\boldsymbol{x}$, evaluated at the equilibrium point $\bar{\boldsymbol{x}}$, such that $\boldsymbol{J}$ can be expressed as follows.

$$\boldsymbol{J} = \frac{\partial \boldsymbol{f}}{\partial \boldsymbol{x}}(\bar{\boldsymbol{x}}) = \begin{bmatrix} \frac{\partial f_1}{\partial x_1}(\bar{\boldsymbol{x}}) & \frac{\partial f_1}{\partial x_2}(\bar{\boldsymbol{x}}) & \cdots & \frac{\partial f_1}{\partial x_n}(\bar{\boldsymbol{x}}) \\ \frac{\partial f_2}{\partial x_1}(\bar{\boldsymbol{x}}) & \frac{\partial f_2}{\partial x_2}(\bar{\boldsymbol{x}}) & \cdots & \frac{\partial f_2}{\partial x_n}(\bar{\boldsymbol{x}}) \\ \vdots & \vdots & \ddots & \vdots \\ \frac{\partial f_n}{\partial x_1}(\bar{\boldsymbol{x}}) & \frac{\partial f_n}{\partial x_2}(\bar{\boldsymbol{x}}) & \cdots & \frac{\partial f_n}{\partial x_n}(\bar{\boldsymbol{x}}) \end{bmatrix}, \tag{4}$$

where $\boldsymbol{J}$ is the Jacobian matrix of the function f at the point $\bar{\boldsymbol{x}}$.

Thus, the linearization of the nonlinear differential equation system around the equilibrium point $\bar{\boldsymbol{x}}$ is given by the following system of differential equations:

$$\dot{\boldsymbol{x}} = \frac{\partial \boldsymbol{f}}{\partial \boldsymbol{x}}(\overline{\boldsymbol{x}})(\boldsymbol{x} - \overline{\boldsymbol{x}}) \,. \tag{5}$$

(Boyce & DiPrima, 2009).

Next Generation Matrix Method

The construction of the Next Generation Matrix (NGM) aims to determine $\mathcal{R}_0$ for an epidemiological model. This method was first introduced by Diekmann et al. in 1990. The NGM is a matrix that corresponds to the number of newly infected individuals in various categories across successive generations. The NGM is typically denoted by $\boldsymbol{K}$, and $\mathcal{R}_0$ is the spectral radius of the matrix $\boldsymbol{K}$. The concept of NGM is divided into three approaches: NGM with a large domain, NGM, and NGM with a small domain**.** However, only the NGM approach will be described below (Diekmann et al., 2010).

The steps required to construct the matrix $\boldsymbol{K}$ are as follows:

1. Linearize the infected subpopulations and substitute the Disease-Free Equilibrium (DFE) point.
2. Perform the decomposition of the Jacobian matrix. The decomposition of the matrix $\boldsymbol{J}|_{DFE}$ must satisfy the following equation:

$$\boldsymbol{J}|_{DFE} = \boldsymbol{T} + \Sigma \,. \tag{6}$$

3. Define the matrix $\boldsymbol{E}$. The conditions for defining the matrix $\boldsymbol{E}$ are as follows:
4. The matrix $\boldsymbol{E}$ must have the same number of rows as the matrix $\boldsymbol{T}$.
5. There must be one column in the matrix $\boldsymbol{E}$ for each row in the matrix $\boldsymbol{T}$ that has non-zero entries. In one column of matrix $\boldsymbol{E}$, there is an entry of 1 corresponding to the non-zero row in matrix $\boldsymbol{T}$, and the remaining entries are zero.
6. Calculate the Next Generation Matrix (NGM), denoted as $\boldsymbol{K}$. The formula for the NGM matrix $\boldsymbol{K}$ is as follows:

$$\boldsymbol{K} = -\boldsymbol{E}^T \boldsymbol{T} \Sigma^{-1} \boldsymbol{E} \tag{7}$$

Definition 6. The spectral radius of the matrix $\boldsymbol{K}$ is defined as the largest or maximum absolute value of the eigenvalues of the matrix, which can be written as follows:

$$\rho(\boldsymbol{K}) = \sup\{|\lambda| : \lambda \in \sigma(\boldsymbol{K})\}, \tag{8}$$

where $\sigma(\boldsymbol{K})$ represents the eigenvalues of the matrix $\boldsymbol{K}$ (Martcheva, 2015).

Van den Driessche and Watmough Approach

The Van den Driessche and Watmough approach is used to analyze the stability of the disease-free equilibrium point in endemic models. Let $x = (x_1, x_2, \dots, x_n)^t$ represent the number of individuals in each compartment, with each $x_i \geq 0$. It is assumed that the first mmm-subpopulations represent the infected individuals. Then, let $\mathcal{F}_i(x)$ be the rate of new infections arising from compartment i, and $\mathcal{V}_i(x) = \mathcal{V}_i^- - \mathcal{V}_i^+$, where $\mathcal{V}_i^-$ is the rate at which individuals transition out

of compartment i, while $\mathcal{V}_i^+$ is the rate at which individuals transition into compartment i. Define $\boldsymbol{X}_s = \{x \geq 0 | x_i,\ \ i = 0,1,2,\dots,m\}$ as the set of disease-free equilibrium points of the model represented by the system of equations (11) as follows:

$$\dot{x}_i = f_i(x) = \mathcal{F}_i(x) - \mathcal{V}_i(x),\ \ i = 1,2,\dots,n \tag{9}$$

If x_0 is the disease-free equilibrium point of the model, then x_0 is locally asymptotically stable if $\mathcal{R}_0 < 1$ and unstable when $\mathcal{R}_0 > 1$, provided that the following five conditions are met:

1. If $x \geq 0$, then $\mathcal{F}_i, \mathcal{V}_i^-, \mathcal{V}_i^+ \geq 0$ for $i = 1,2,\dots,n$.
2. If $x_i = 0$, then $\mathcal{V}_i^- = 0$. Specifically, if $\in \boldsymbol{X}_s$, then $\mathcal{V}_i^- = 0$ for $\mathcal{V}_i^- = 0$ untuk $i = 1,2,\dots,m$.
3. If $i > m$, then $\mathcal{F}_i = 0$.
4. If $\in \boldsymbol{X}_s$, then $\mathcal{F}_i(x) = 0$ and $\mathcal{V}_i^+ = 0$ for $i = 1,2,\dots,m$.
5. If $\mathcal{F}(x) = 0$, then all eigenvalues of $Df(x_0)$ are real and negative, where $Df(x_0)$ is the Jacobian matrix of the linearized nonlinear system of differential equations (9) evaluated at the disease-free equilibrium point.

(Van Den Driessche & Watmough, 2002).

Elasticity Analysis

Definition 7. If $\mathcal{Q}$ is a function that can be differentiated with respect to its parameters, then the elasticity analysis of the percentage change in all parameters p is formulated as follows:

$$\mathcal{E}_{\partial\mathcal{Q}}^{p} = \frac{\partial\mathcal{Q}}{\partial p} \times \frac{p}{\mathcal{Q}} \approx \frac{\%\Delta\mathcal{Q}}{\%\Delta p}. \tag{10}$$

(Chitnis et al., 2008).

RESULTS AND DISCUSSION

One-Way Mobility Model

The one-way mobility model describes a situation in which only one of the two cities exhibits high mobility. In this case, a portion of the population from that city not only engages in activities within their own city but also commutes and performs activities in the other city. Conversely, the population in the other city is characterized by low mobility, meaning that individuals only carry out activities within their own city without traveling elsewhere.

The construction of the model rests on the following assumptions. First, the population of each city is well mixed, so that within-city transmission follows the law of mass action and every susceptible individual is equally likely to contact any infectious individual. Second, each population is open: individuals enter through a constant recruitment rate and leave through natural death, while infected individuals are additionally subject to disease-induced death. Third, the course of infection is divided into exposed, asymptomatic, and symptomatic stages, and both

asymptomatic and symptomatic individuals are capable of transmitting the disease. Fourth, mobility is strictly unidirectional: only one city (City 2) contains a high-mobility subpopulation that also performs activities in the other city, whereas the first city generates no outward movement, so that only the second city contributes a nonzero proportion of highly mobile individuals. Fifth, all epidemiological parameters are assumed constant over the simulation horizon, so that the resulting system is autonomous and its long-term behavior is governed by its equilibrium points.

The parameter values used in the elasticity analysis and numerical simulations are adopted from the no-mobility study of (Balya et al., 2025) and from representative ranges reported in the COVID-19 modelling literature, while the mobility-related values are selected so as to realize each of the three scenarios considered below. Because the present study focuses on the qualitative effect of directed movement rather than on forecasting a specific outbreak, the model is not calibrated to a particular empirical data set; formal calibration and validation against region-specific surveillance data are identified as an important direction for future work.

This mobility pattern is represented by the proportion of highly mobile individuals, denoted as P_1 for city 1 and P_2 for city 2, while the proportion of low-mobility individuals is given by $(1-P_1)$ and $(1-P_2)$ for each respective city. To construct the one-way mobility model, it is assumed that only one city has a highly mobile population. In this section, we set $P_1 = 0$ and $P_2 \neq 0$, and the one-way mobility model is then formulated as follows:

$$\begin{aligned}
\frac{dS_1}{dt} &= \Lambda_1 - \beta_1 S_1 A_1 - \beta_1 S_1 P_2 A_2 - \mu S_1 , \\
\frac{dE_1}{dt} &= \beta_1 S_1 A_1 + \beta_1 S_1 P_2 A_2 - q_1 \alpha E_1 - (1-q_1)\alpha E_1 - \mu E_1 , \\
\frac{dA_1}{dt} &= q_1 \alpha E_1 - \delta A_1 - \gamma A_1 - \mu A_1 - \xi A_1 , \\
\frac{dI_1}{dt} &= (1-q_1)\alpha E_1 + \delta A_1 - \eta_1 I_1 - \mu I_1 - \xi I_1 , \\
\frac{dR_1}{dt} &= \gamma A_1 + \eta_1 I_1 - \mu R_1 ,
\end{aligned}$$

for city 1 and

$$\begin{aligned}
\frac{dS_2}{dt} &= \Lambda_2 - \beta_2 S_2 A_2 - \beta_1 A_1 P_2 S_2 - \mu S_2 , \\
\frac{dE_2}{dt} &= \beta_2 S_2 A_2 + \beta_1 A_1 P_2 S_2 - q_2 \alpha E_2 - (1-q_2)\alpha E_2 - \mu E_2 , \\
\frac{dA_2}{dt} &= q_2 \alpha E_2 - \delta A_2 - \gamma A_2 - \mu A_2 - \xi A_2 , \\
\frac{dI_2}{dt} &= (1-q_2)\alpha E_2 + \delta A_2 - \eta_2 I_2 - \mu I_2 - \xi I_2 , \\
\frac{dR_2}{dt} &= \gamma A_2 + \eta_2 I_2 - \mu R_2 ,
\end{aligned} \tag{11}$$

for city 2.

Table 1. Description of Model Variables Given in Systems (1)

Variables	Description
S_1	The number of people in city 1 who are vulnerable to COVID-19
E_1	The number of people in city 1 who are infected with COVID-19 but have not yet transmitted the disease
A_1	The number of people in city 1 who are infected with COVID-19 but asymptomatic and undetected
I_1	The number of people in city 1 infected with COVID-19 showing symptoms and detected
R_1	The number of people in city 1 who have recovered from COVID-19
S_2	The number of people in city 2 who are vulnerable to COVID-19
E_2	The number of people in city 2 who are infected with COVID-19 but have not yet transmitted the disease
A_2	The number of people in city 2 who are infected with COVID-19 but asymptomatic and undetected
I_2	The number of people in city 2 infected with COVID-19 showing symptoms and detected
R_2	The number of people in city 2 who have recovered from COVID-19

The table below presents the parameters in the model along with their descriptions and estimated values.

Table 2. Model Parameters with Their Descriptions and Estimated Values

Variables	Description	Values	Source
Λ_1	Human recruitment rate in city 1	$10^7/(70 \times 365)$	(Aldila et al., 2020)
Λ_2	Human recruitment rate in city 2	$10^7/(70 \times 365)$	(Aldila et al., 2020)
β_1	Rate of transmission of susceptible individuals in city 1	1.85×10^{-7}	(Balya et al., 2021)
β_2	Rate of transmission of susceptible individuals in city 2	8.3×10^{-8}	(Balya et al., 2021)
μ	Natural death rate	$1/(70 \times 365)$	(Feng & Velasco, 1997)
q_1	The proportion of people in city 1 who are exposed to COVID-19 and then move to A_1	0.5	estimated
q_2	The proportion of people in city 2 who are exposed to COVID-19 and then move to A_2	0.5	estimated
$1-q_1$	The proportion of people in city 1 who are exposed to COVID-19 and then move to I_1	0.5	estimated
$1-q_2$	The proportion of people in city 2 who are exposed	0.5	estimated

Variables	Description	Values	Source
	to COVID-19 and then move to I_2		
α	Incubation Rate	$1/5.1$	(Li et al., 2020)
δ	The rate of human movement from A_1 to I_1 and A_2 to I_2	0.01	estimated
ξ	Death rate due to COVID-19	0.05	(Aldila et al., 2021)
η_1	The Recovery rate of the I_1 subpopulation in city 1	0.1	estimated
η_2	The Recovery rate of the I_2 subpopulation in city 2	0.125	estimated
γ	The Recovery rate of the A_1 and A_2 subpopulation	0.1	(Balya et al., 2025)
P_2	The proportion of highly mobile susceptible individuals in city 2	[0,1]	estimated

Model Analysis

The disease-free equilibrium (DFE) of COVID-19 for the one-way mobility model in system (11) can be obtained when the numbers of exposed and infected individuals are zero; that is, the numbers of exposed, infected-asymptomatic, and infected-symptomatic individuals in both City 1 and City 2 satisfy $E_1 = 0, E_2 = 0, A_1 = 0, A_2 = 0, I_1 = 0, I_2 = 0$. By substituting these values into the compartments $\frac{dS_1}{dt}$, $\frac{dS_2}{dt}$, $\frac{dR_1}{dt}$, and $\frac{dR_2}{dt}$ in system (11), the corresponding values of S_1, R_1, S_2, and R_2 can be obtained, and the DFE is then determined. Thus, the disease-free equilibrium for the COVID-19 transmission model with one-way mobility in system (11) is obtained as follows:

$$\begin{aligned} DFE &= (S_1^0, E_1^0, A_1^0, I_1^0, R_1^0, S_2^0, E_2^0, A_2^0, I_2^0, R_2^0) \\ &= \left(\frac{\Lambda_1}{\mu}, 0,0,0,0, \frac{\Lambda_2}{\mu}, 0,0,0,0\right). \end{aligned} \tag{12}$$

After obtaining the disease-free equilibrium (DFE), the next step is to determine the basic reproduction number, denoted by $\mathcal{R}_0$. The value of $\mathcal{R}_0$ can be derived using the Next Generation Matrix (NGM) approach. The NGM is a matrix that corresponds to the number of newly infected individuals in various categories across successive generations (Diekmann et al., 2010). The first step in constructing the NGM is to linearize all subpopulations exposed to and infected with the disease in both City 1 and City 2 $(E_1, E_2, A_1, A_2, I_1, I_2)$ from system (11), resulting in the Jacobian matrix shown in equation (13) below.

$$\mathcal{J} = \begin{bmatrix} j_{11} & \beta_1 S_1 & 0 & 0 & j_{15} & 0 \\ q_1\alpha & j_{22} & 0 & 0 & 0 & 0 \\ (1-q_1)\alpha & \delta & -\eta_1-\mu-\xi & 0 & 0 & 0 \\ 0 & j_{42} & 0 & j_{44} & \beta_2 S_2 & 0 \\ 0 & 0 & 0 & q_2\alpha & j_{55} & 0 \\ 0 & 0 & 0 & (1-q_2)\alpha & \delta & -\eta_2-\mu-\xi \end{bmatrix}, \quad (13)$$

with
$j_{11} = -q_1\alpha - (1-q_1)\alpha - \mu$,
$j_{15} = \beta_1 P_2 S_1$,
$j_{22} = j_{55} = -\delta - \gamma - \mu - \xi$,
$j_{42} = \beta_1 P_2 S_2$,
$j_{44} = -q_2\alpha - (1-q_2)\alpha - \mu$.

Next, the Jacobian matrix in equation (13) is decomposed as $J = T + \Sigma$. Here, T is the transmission matrix associated with the process of disease transmission or new infections, while Σ is the transition matrix associated with the movement of individuals among the exposed and infected compartments. By substituting the DFE into the transmission matrix $T$and the transition matrix Σ, we obtain:

$$\mathcal{T}_{|DFE} = \begin{bmatrix} 0 & \frac{\Lambda_1\beta_1}{\mu} & 0 & 0 & \frac{\Lambda_1\beta_1 P_2}{\mu} & 0 \\ 0 & 0 & 0 & 0 & 0 & 0 \\ 0 & 0 & 0 & 0 & 0 & 0 \\ 0 & \frac{\Lambda_2\beta_1 P_2}{\mu} & 0 & 0 & \frac{\Lambda_2\beta_2}{\mu} & 0 \\ 0 & 0 & 0 & 0 & 0 & 0 \\ 0 & 0 & 0 & 0 & 0 & 0 \end{bmatrix} \text{ and}$$

$$\boldsymbol{\Sigma}_{|DFE} = \quad (14)$$

$$\begin{bmatrix} j_{11} & 0 & 0 & 0 & 0 & 0 \\ q_1\alpha & j_{22} & 0 & 0 & 0 & 0 \\ (1-q_1)\alpha & \delta & -\eta_1-\mu-\xi & 0 & 0 & 0 \\ 0 & 0 & 0 & j_{44} & 0 & 0 \\ 0 & 0 & 0 & q_2\alpha & j_{55} & 0 \\ 0 & 0 & 0 & (1-q_2)\alpha & \delta & -\eta_2-\mu-\xi \end{bmatrix},$$

with
$j_{11} = -q_1\alpha - (1-q_1)\alpha - \mu$,
$j_{22} = j_{55} = -\delta - \gamma - \mu - \xi$,
$j_{44} = -q_2\alpha - (1-q_2)\alpha - \mu$.

Next, the Next Generation Matrix (NGM), denoted by K, is computed using the following procedure:

$$\boldsymbol{\mathcal{K}} = -\boldsymbol{E}^T . \boldsymbol{\mathcal{T}}_{|DFE} . \boldsymbol{\Sigma}_{|DFE}^{-1} . \boldsymbol{E}$$

with

$$\boldsymbol{E} = \begin{bmatrix} 1 & 0 \\ 0 & 0 \\ 0 & 0 \\ 0 & 1 \\ 0 & 0 \\ 0 & 0 \end{bmatrix} \text{ and } \boldsymbol{E}^T = \begin{bmatrix} 1 & 0 & 0 & 0 & 0 & 0 \\ 0 & 0 & 0 & 1 & 0 & 0 \end{bmatrix}$$

Hence, the resulting matrix $\boldsymbol{\mathcal{K}}$ can be expressed as follows:

$$\boldsymbol{\mathcal{K}} = \begin{bmatrix} k_{11} & k_{12} \\ k_{21} & k_{22} \end{bmatrix},$$

with

$k_{11} = \frac{\Lambda_1 \beta_1 q_1 \alpha}{\mu(\delta+\gamma+\mu+\xi)(\alpha+\mu)}$,

$k_{12} = \frac{\Lambda_1 \beta_1 P_2 q_2 \alpha}{\mu(\delta+\gamma+\mu+\xi)(\alpha+\mu)}$,

$k_{21} = \frac{\Lambda_2 \beta_1 P_2 q_1 \alpha}{\mu(\delta+\gamma+\mu+\xi)(\alpha+\mu)}$,

$k_{22} = \frac{\Lambda_2 \beta_2 q_2 \alpha}{\mu(\delta+\gamma+\mu+\xi)(\alpha+\mu)}$.

Subsequently, the characteristic polynomial corresponding to the matrix $\boldsymbol{\mathcal{K}}$ is derived as follows:

$$\lambda^2 - \frac{(\Lambda_1 \beta_1 q_1 + \Lambda_2 \beta_2 q_2)\alpha}{\mu(\delta+\gamma+\mu+\xi)(\alpha+\mu)}\lambda - \frac{\Lambda_1 \beta_1 q_1 \Lambda_2 q_2 \alpha^2}{\mu^2(\delta+\gamma+\mu+\xi)^2(\alpha+\mu)^2}(P_2^2\beta_1 - \beta_2) = 0$$

Next, the basic reproduction number $\mathcal{R}_0$ is obtained by determining the dominant eigenvalue of the matrix $\boldsymbol{\mathcal{K}}$. This yields two eigenvalues as follows:

$$\lambda_1 = \frac{\left(\Lambda_1\beta_1 q_1 + \Lambda_2\beta_2 q_2 + \sqrt{4\Lambda_1\Lambda_2 P_2^2 \beta_1^2 q_1 q_2 - 2\Lambda_1\Lambda_2\beta_1\beta_2 q_1 q_2 + \Lambda_1^2\beta_1^2 q_1^2 + \Lambda_2^2\beta_2^2 q_2^2}\right)\alpha}{2(\delta+\gamma+\mu+\xi)(\alpha+\mu)\mu},$$

$$\lambda_2 = \frac{\left(\Lambda_1\beta_1 q_1 + \Lambda_2\beta_2 q_2 - \sqrt{4\Lambda_1\Lambda_2 P_2^2 \beta_1^2 q_1 q_2 - 2\Lambda_1\Lambda_2\beta_1\beta_2 q_1 q_2 + \Lambda_1^2\beta_1^2 q_1^2 + \Lambda_2^2\beta_2^2 q_2^2}\right)\alpha}{2(\delta+\gamma+\mu+\xi)(\alpha+\mu)\mu}.$$

Since λ_1 is the largest eigenvalue, it represents the basic reproduction number $\mathcal{R}_0$ for the COVID-19 transmission model with one-way mobility. Thus, $\mathcal{R}_0$ can be expressed as follows:

$$\mathcal{R}_0^{one-way\,(2\to1)} = \frac{\left(\Lambda_1\beta_1 q_1 + \Lambda_2\beta_2 q_2 + \sqrt{4\Lambda_1\Lambda_2 P_2^2 \beta_1^2 q_1 q_2 - 2\Lambda_1\Lambda_2\beta_1\beta_2 q_1 q_2 + \Lambda_1^2\beta_1^2 q_1^2 + \Lambda_2^2\beta_2^2 q_2^2}\right)\alpha}{2(\delta+\gamma+\mu+\xi)(\alpha+\mu)\mu}. \quad (15)$$

Theorem 1. *The COVID-19 transmission model with one-way mobility in system (11) has a basic reproduction number, $\mathcal{R}_0^{one-way\,(2\to1)}$, which is given in equation (15).*

The stability property of the DFE for this model can then be determined using Theorem 2. presented below.

Theorem 2. *The disease-free equilibrium of the COVID-19 transmission model with one-way mobility in system (11) is locally asymptotically stable if $\mathcal{R}_0^{one-way\,(2\to1)} < 1$, and unstable if $\mathcal{R}_0^{one-way\,(2\to1)} > 1$.*

Proof. First, system (11) is rearranged by placing the m −infected compartments at the beginning, followed by the uninfected compartments. After this reordering, the system can be expressed as equation (16) below.

$$
\begin{aligned}
f_1 &= \frac{dE_1}{dt} = \beta_1 S_1 A_1 + \beta_1 S_1 P_2 A_2 - q_1 \alpha E_1 - (1-q_1)\alpha E_1 - \mu E_1 , \\
f_2 &= \frac{dA_1}{dt} = q_1 \alpha E_1 - \delta A_1 - \gamma A_1 - \mu A_1 - \xi A_1 , \\
f_3 &= \frac{dI_1}{dt} = (1-q_1)\alpha E_1 + \delta A_1 - \eta_1 I_1 - \mu I_1 - \xi I_1 , \\
f_4 &= \frac{dE_2}{dt} = \beta_2 S_2 A_2 + \beta_1 A_1 P_2 S_2 - q_2 \alpha E_2 - (1-q_2)\alpha E_2 - \mu E_2 , \\
f_5 &= \frac{dA_2}{dt} = q_2 \alpha E_2 - \delta A_2 - \gamma A_2 - \mu A_2 - \xi A_2 , \\
f_6 &= \frac{dI_2}{dt} = (1-q_2)\alpha E_2 + \delta A_2 - \eta_2 I_2 - \mu I_2 - \xi I_2 , \\
f_7 &= \frac{dR_1}{dt} = \gamma A_1 + \eta_1 I_1 - \mu R_1 , \\
f_8 &= \frac{dR_2}{dt} = \gamma A_2 + \eta_2 I_2 - \mu R_2 , \\
f_9 &= \frac{dS_1}{dt} = \Lambda_1 - \beta_1 S_1 A_1 - \beta_1 S_1 P_2 A_2 - \mu S_1 , \\
f_{10} &= \frac{dS_2}{dt} = \Lambda_2 - \beta_2 S_2 A_2 - \beta_1 A_1 P_2 S_2 - \mu S_2 .
\end{aligned} \tag{16}
$$

Next, the set $\boldsymbol{X_s}$ is defined as the disease-free state, in which all infected compartments are equal to zero, while the susceptible compartments take values determined by the recruitment and mortality rates. This set is given by:

$$
\begin{aligned}
\mathbf{X_s} = \Big\{ & x_1 = E_1 = 0, x_2 = A_1 = 0, x_3 = I_1 = 0, x_4 = E_2 = 0, x_5 = A_2 = 0, x_6 = I_2 \\
& = 0, x_7 = R_1 = 0, x_8 = R_2 = 0, x_9 = S_1 = \frac{\Lambda_1}{\mu}, x_{10} = S_2 = \frac{\Lambda_2}{\mu} \Big\}.
\end{aligned}
$$

In this disease transmission model, the initial conditions of each compartment must be non-negative and must satisfy the following system of equations:

$$\dot{x}_i = f_i(x) = \mathcal{F}_i(x) - \mathcal{V}_i(x), \qquad i = 1,2,\dots,n , \tag{17}$$

where n denotes the total number of compartments, and $\mathcal{V}_i = \mathcal{V}_i^- - \mathcal{V}_i^+$.

It should be noted that $\mathcal{F}_i$ represents the rate of new infections arising in the i −th compartment, while $\mathcal{V}_i^-$ denotes the rate at which individuals leave that compartment, and $\mathcal{V}_i^+$ describes the rate at which individuals enter the i −th compartment. Based on these definitions, the explicit forms of $\mathcal{F}_i(x)$, $\mathcal{V}_i^-(x)$, and $\mathcal{V}_i^+(x)$ can be written as follows:

$$
\mathcal{F}_i(x) = \begin{bmatrix} \beta_1 S_1 A_1 + \beta_1 S_1 P_2 A_2 \\ 0 \\ 0 \\ \beta_2 S_2 A_2 + \beta_1 A_1 P_2 S_2 \\ 0 \\ 0 \\ 0 \\ 0 \\ 0 \\ 0 \end{bmatrix}, \tag{18}
$$

$$\mathcal{V}_i^- = \begin{bmatrix} q_1\alpha E_1 + (1-q_1)\alpha E_1 + \mu E_1 \\ \delta A_1 + \gamma A_1 + \mu A_1 + \xi A_1 \\ \eta_1 I_1 + \mu I_1 + \xi I_1 \\ q_2\alpha E_2 + (1-q_2)\alpha E_2 + \mu E_2 \\ \delta A_2 + \gamma A_2 + \mu A_2 + \xi A_2 \\ \eta_2 I_2 + \mu I_2 + \xi I_2 \\ \mu R_1 \\ \mu R_2 \\ \beta_1 S_1 A_1 + \beta_1 S_1 P_2 A_2 + \mu S_1 \\ \beta_2 S_2 A_2 + \beta_1 A_1 P_2 S_2 + \mu S_2 \end{bmatrix}, \tag{19}$$

and

$$\mathcal{V}_i^+ = \begin{bmatrix} 0 \\ q_1\alpha E_1 \\ (1-q_1)\alpha E_1 + \delta A_1 \\ 0 \\ q_2\alpha E_2 \\ (1-q_2)\alpha E_2 + \delta A_2 \\ \gamma A_1 + \eta_1 I_1 \\ \gamma A_2 + \eta_2 I_2 \\ \Lambda_1 \\ \Lambda_2 \end{bmatrix}. \tag{20}$$

The stability analysis of the DFE can then be carried out by verifying conditions 1 – 5, which are stated below.

1. If $x \geq 0$, then $\mathcal{F}_i, \mathcal{V}_i^-, \mathcal{V}_i^+ \geq 0$ for $i = 1,2,\dots,n$. From equations (18)–(20), all parameters and variables are non-negative, so $\mathcal{F}_i$, $\mathcal{V}_i^-$, $\mathcal{V}_i^+ \geq 0$. Thus, condition 1 is satisfied**.**
2. If a subpopulation is empty, no individuals leave the compartment. Therefore, $x_i = 0 \Rightarrow \mathcal{V}_i^- = 0$. For $x \in \mathbf{X_s}$ and $i = 1,\dots,m$ where m is the number of infected compartments (the number of non-infected compartments is not involved), and then substituting $x_i = 0$ into $\mathcal{V}_i^-(x)$ yields:

$$\mathcal{V}_i^- = \begin{bmatrix} 0 \\ 0 \\ 0 \\ 0 \\ 0 \\ 0 \end{bmatrix}.$$

   Hence all entries are zero, and condition 2 is satisfied**.**
3. A disease-free subpopulation cannot generate new infections: $\mathcal{F}_i = 0$, for $i > m$. Since the population is assumed to be closed (no immigration), so based on equation (18) for $i = 7,8,9,10$ (considering only the non-infected compartments) gives: $\mathcal{F}_7(x) = 0$, $\mathcal{F}_8(x) = 0$, $\mathcal{F}_9(x) = 0$, $\mathcal{F}_{10}(x) = 0$. Therefore, condition 3 is satisfied**.**
4. For the disease-free state $x \in \mathbf{X_s}$, the infected compartments satisfy: $\mathcal{F}_i(x) = 0$ and $\mathcal{V}_i^+(x) = 0$, for $i = 1,2,\dots,m$. Substituting $x_i = 0$ into

equations (18) and equation (20) for $i = 1,2,3,4,5,6$ (considering only the infected compartments) gives:

$$\mathcal{F}_i = \begin{bmatrix} 0 \\ 0 \\ 0 \\ 0 \\ 0 \\ 0 \end{bmatrix} \text{ and } \mathcal{V}_i^+ = \begin{bmatrix} 0 \\ 0 \\ 0 \\ 0 \\ 0 \\ 0 \end{bmatrix}.$$

5. If $\mathcal{F}(x) = 0$, then all eigenvalues of the Jacobian matrix $Df(x_0)$ have negative real parts, where x_0 is the disease-free equilibrium (DFE). By setting $\mathcal{F}(x) = 0$, the model reduces to a system without new infections, given by equation (21) below.

$$\begin{aligned}
f_1 &= \frac{dE_1}{dt} = -q_1\alpha E_1 - (1-q_1)\alpha E_1 - \mu E_1 , \\
f_2 &= \frac{dA_1}{dt} = q_1\alpha E_1 - \delta A_1 - \gamma A_1 - \mu A_1 - \xi A_1 , \\
f_3 &= \frac{dI_1}{dt} = (1-q_1)\alpha E_1 + \delta A_1 - \eta_1 I_1 - \mu I_1 - \xi I_1 , \\
f_4 &= \frac{dE_2}{dt} = -q_2\alpha E_2 - (1-q_2)\alpha E_2 - \mu E_2 , \\
f_5 &= \frac{dA_2}{dt} = q_2\alpha E_2 - \delta A_2 - \gamma A_2 - \mu A_2 - \xi A_2 , \\
f_6 &= \frac{dI_2}{dt} = (1-q_2)\alpha E_2 + \delta A_2 - \eta_2 I_2 - \mu I_2 - \xi I_2 , \\
f_7 &= \frac{dR_1}{dt} = \gamma A_1 + \eta_1 I_1 - \mu R_1 , \\
f_8 &= \frac{dR_2}{dt} = \gamma A_2 + \eta_2 I_2 - \mu R_2 , \\
f_9 &= \frac{dS_1}{dt} = \Lambda_1 - \beta_1 S_1 A_1 - \beta_1 S_1 P_2 A_2 - \mu S_1 , \\
f_{10} &= \frac{dS_2}{dt} = \Lambda_2 - \beta_2 S_2 A_2 - \beta_1 A_1 P_2 S_2 - \mu S_2 .
\end{aligned} \tag{21}$$

Next, linearization is performed and the disease-free equilibrium (DFE) is substituted in order to obtain the Jacobian matrix, which is given as follows:

$$\mathcal{D}f(x_0) = \begin{bmatrix} A_{11}^0 & A_{12}^0 & A_{13}^0 & A_{14}^0 & A_{15}^0 \\ A_{21}^0 & A_{22}^0 & A_{23}^0 & A_{24}^0 & A_{25}^0 \\ A_{31}^0 & A_{32}^0 & A_{33}^0 & A_{34}^0 & A_{35}^0 \\ A_{41}^0 & A_{42}^0 & A_{43}^0 & A_{44}^0 & A_{45}^0 \\ A_{51}^0 & A_{52}^0 & A_{53}^0 & A_{54}^0 & A_{55}^0 \end{bmatrix}, \tag{22}$$

with

$$A_{11}^0 = \begin{bmatrix} -q_1\alpha - (1-q_1)\alpha - \mu & 0 \\ q_1\alpha & -\delta - \gamma - \mu - \xi \end{bmatrix},$$

$$A_{21}^0 = \begin{bmatrix} (1-q_1)\alpha & \delta \\ 0 & 0 \end{bmatrix},$$

$$A_{22}^0 = \begin{bmatrix} -\eta_1 - \mu - \xi & 0 \\ 0 & -q_2\alpha - (1-q_2)\alpha - \mu \end{bmatrix},$$
$$A_{32}^0 = \begin{bmatrix} 0 & q_2\alpha \\ 0 & (1-q_2)\alpha \end{bmatrix},$$
$$A_{33}^0 = \begin{bmatrix} -\delta - \gamma - \mu - \xi & 0 \\ \delta & -\eta_2 - \mu - \xi \end{bmatrix},$$
$$A_{41}^0 = \begin{bmatrix} 0 & \gamma \\ 0 & 0 \end{bmatrix},$$
$$A_{42}^0 = \begin{bmatrix} \eta_1 & 0 \\ 0 & 0 \end{bmatrix},$$
$$A_{43}^0 = \begin{bmatrix} 0 & 0 \\ \gamma & \eta_2 \end{bmatrix},$$
$$A_{51}^0 = \begin{bmatrix} 0 & \dfrac{-\Lambda_1\beta_1}{\mu} \\ 0 & -\dfrac{\Lambda_2\beta_1 P_2}{\mu} \end{bmatrix},$$
$$A_{53}^0 = \begin{bmatrix} -\dfrac{\Lambda_1\beta_1 P_2}{\mu} & 0 \\ -\dfrac{\Lambda_2\beta_2}{\mu} & 0 \end{bmatrix},$$
$$A_{44}^0 = A_{55}^0 = \begin{bmatrix} -\mu & 0 \\ 0 & -\mu \end{bmatrix},$$
$$A_{12}^0 = A_{13}^0 = A_{14}^0 = A_{15}^0 = A_{23}^0 = A_{24}^0 = A_{25}^0 = A_{31}^0 = A_{34}^0 = A_{35}^0 = A_{45}^0 = A_{52}^0 = A_{54}^0 = \begin{bmatrix} 0 & 0 \\ 0 & 0 \end{bmatrix}.$$

Thus, the characteristic polynomial is obtained as

$$(\lambda+\mu)^4(\lambda+\alpha+\mu)^2(\lambda+\delta+\gamma+\mu+\xi)^2(\lambda+\eta_1+\mu+\xi)$$
$$(\lambda+\eta_2+\mu+\xi) = 0\,.$$

and it can be verified that all eigenvalues are negative. Therefore, condition 5 is satisfied.

Since all Conditions 1–5 are fulfilled, Theorem 2 is proven. In other words, the disease-free equilibrium of the COVID-19 transmission model with one-way mobility in system (11) is locally asymptotically stable if $\mathcal{R}_0^{one-way\,(2\to1)} < 1$, and unstable if $\mathcal{R}_0^{one-way\,(2\to1)} > 1$. ■

Discussion of the One-Way Mobility Model

The Next Generation Matrix (NGM) successfully captures the number of new infections based on location and case type. In the matrix $\mathcal{K}$, each entry represents a parameter component with its own epidemiological meaning. The first row and first column entry, given by $k_{11} = \frac{\Lambda_1\beta_1 q_1\alpha}{\mu(\delta+\gamma+\mu+\xi)(\alpha+\mu)}$ represents the number of new infections in City 1 caused by individuals from City 1. Similarly, the second row and second column entry, $k_{22} = \frac{\Lambda_2\beta_2 q_2\alpha}{\mu(\delta+\gamma+\mu+\xi)(\alpha+\mu)}$, represents the number of new infections in City 2 caused by individuals from City 2. The first row and second column entry, $k_{12} = \frac{\Lambda_1\beta_1 P_2 q_2\alpha}{\mu(\delta+\gamma+\mu+\xi)(\alpha+\mu)}$, represents the number of new infections in

City 1 caused by individuals from City 2 who engage in social activities in City 1. Finally, the second row and first column entry, $k_{21} = \frac{\Lambda_2\beta_1 P_2 q_1 \alpha}{\mu(\delta+\gamma+\mu+\xi)(\alpha+\mu)}$, represents the number of new infections in City 2 arising from individuals with high mobility, a situation commonly referred to as imported disease.

After that, from the matrix $\mathcal{K}$ above, the characteristic polynomial is obtained as follows:

$$\underbrace{\lambda^2 - a_1\lambda}_{z_1} \quad - \quad \underbrace{a_0(P_2^2\beta_1 - \beta_2)}_{z_2} = 0$$

where

$a_1 = \frac{(\Lambda_1\beta_1 q_1 + \Lambda_2\beta_2 q_2)\alpha}{\mu(\delta+\gamma+\mu+\xi)(\alpha+\mu)} > 0$ and

$a_0 = \frac{\Lambda_1\beta_1 q_1 \Lambda_2 q_2 \alpha^2}{\mu^2(\delta+\gamma+\mu+\xi)^2(\alpha+\mu)^2} > 0$

Consider the polynomial in the component z_1. This corresponds to the polynomial $\lambda^2 - a_1\lambda$. The curve of the characteristic roots of this polynomial can be illustrated in Figure 1 below.

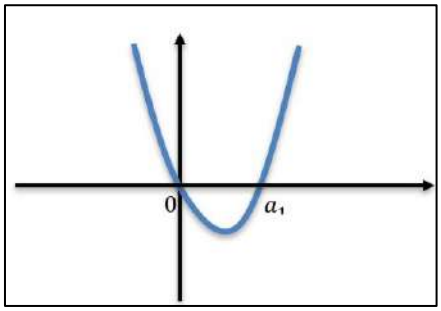

Figure 1. Curve of the Characteristic Roots of the Polynomial $\lambda^2 - a_1\lambda = 0$

Then, when z_1 is reduced by z_2, the curve of the characteristic roots of the polynomial changes. There are two possible curve behaviors when subtracting the component $z_2 = a_0(P_2^2\beta_1 - \beta_2)$. First, if $P_2^2\beta_1 - \beta_2 > 0$, then the curve of the characteristic roots of the polynomial $\lambda^2 - a_1\lambda - a_0(P_2^2\beta_1 - \beta_2)$ is illustrated in Figure 2 below.

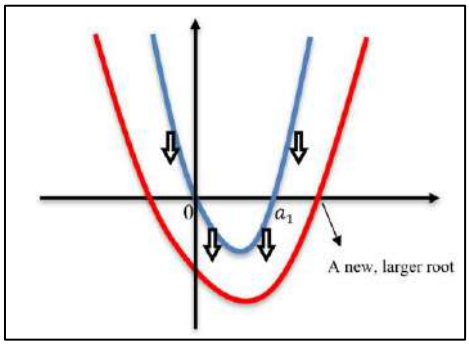

Figure 2. Curve of the Characteristic Roots of the Polynomial $\lambda^2 - a_1\lambda - a_0(P_2^2\beta_1 - \beta_2) = 0$ if $P_2^2\beta_1 - \beta_2 > 0$

Second, if $P_2^2\beta_1 - \beta_2 < 0$, then the curve of the characteristic polynomial $\lambda^2 - a_1\lambda - a_0(P_2^2\beta_1 - \beta_2)$ is illustrated in Figure 3 below.

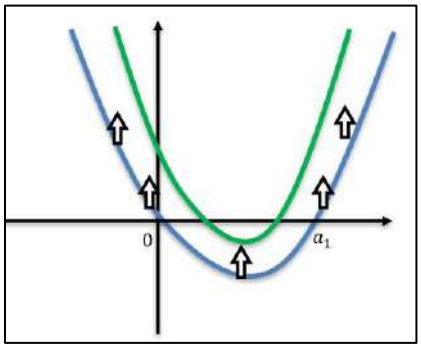

Figure 3. Curve of the Characteristic Roots of the Polynomial $\lambda^2 - a_1\lambda - a_0(P_2^2\beta_1 - \beta_2) = 0$ if $P_2^2\beta_1 - \beta_2 < 0$

The intersection points of each curve represent the value of $\mathcal{R}_0$, and the largest eigenvalue corresponds to the actual $\mathcal{R}_0$. The differences between the curves arise from the term $(P_2^2\beta_1 - \beta_2)$, which serves as a threshold determining whether the arrival of individuals from City 2 to City 1 poses a risk to the population.

If $P_2^2\beta_1 - \beta_2 > 0 \Leftrightarrow \frac{\beta_2}{\beta_1} < P_2^2$, then $\mathcal{R}_0$ increases. This is consistent with Figure 2, which shows the emergence of a larger root compared to Figure 1. Thus, one-way mobility (from City 2 to City 1) significantly influences the endemic level in both cities, and the condition $\frac{\beta_2}{\beta_1} < P_2^2$ indicates a potentially harmful situation for the population. To prevent this condition, one may:

1. Reduce P_2, related to implementing lockdown or movement restrictions.
2. Increase the ratio β_2/β_1 by increasing β_2 or decreasing β_1. However, increasing β_2 would raise the infection rate in City 2, which would clearly endanger the population. Therefore, the alternative approach is to reduce β_1, which corresponds to implementing social distancing measures.

Elasticity Analysis of $\mathcal{R}_0$ in the One-Way Mobility Model

Before analyzing the effect of one-way mobility on the basic reproduction number, it is important to recall that the reproduction number without mobility, denoted by $\mathcal{R}_0^{no\ mobility}$, has been established in a previous study by (Balya et al., 2025) as

$$\mathcal{R}_0^{no\ mobility} = \frac{\Lambda_i\beta_i q_i\alpha}{\mu(\delta+\gamma+\mu+\xi)(\alpha+\mu)}, i = 1,2.$$

These values describe the transmission potential in each city when no movement of individuals occurs between them. In the present study, elasticity analysis is used to examine how one-way mobility (from City 2 to City 1) alters the value of $\mathcal{R}_0^{one-way\ (2\to1)}$. Since the mobility flow occurs only in one direction, the resulting reproduction number depends on the relative magnitudes of the no-mobility reproduction numbers in the two cities, $\mathcal{R}_0^{no\ mobility(1)}$ and $\mathcal{R}_0^{no\ mobility(2)}$.

Because these two values can be ordered in three distinct ways, the elasticity analysis naturally leads to three scenarios:

1. $\mathcal{R}_0^{no\ mobility(1)} > \mathcal{R}_0^{no\ mobility(2)} > 1$
2. $\mathcal{R}_0^{no\ mobility(1)} > 1 > \mathcal{R}_0^{no\ mobility(2)}$
3. $\mathcal{R}_0^{no\ mobility(2)} > 1 > \mathcal{R}_0^{no\ mobility(1)}$

These scenarios represent all possible epidemiological configurations regarding the relative endemicity levels of City 1 and City 2 prior to introducing mobility. By evaluating how each configuration affects $\mathcal{R}_0^{one-way\ (2\to1)}$, we can assess how mobility amplifies or reduces the transmission risk in both cities.

Scenario 1: $\boldsymbol{\mathcal{R}_0^{no\ mobility(1)} > \mathcal{R}_0^{no\ mobility(2)} > 1}$

In this scenario, the parameter values are substituted into the elasticity equations for each parameter with respect to $\mathcal{R}_0^{one-way\ (2\to1)}$ such that the condition $\mathcal{R}_0^{no\ mobility(1)} > \mathcal{R}_0^{no\ mobility(2)} > 1$ is satisfied. The results obtained from this scenario are $\mathcal{R}_0^{no\ mobility(1)} = 2.681711$ and $\mathcal{R}_0^{no\ mobility(2)} = 2.0359$. Under this condition, the resulting value of $\mathcal{R}_0^{one-way\ (2\to1)}$ becomes higher than both, $\mathcal{R}_0^{no\ mobility(1)}$and $\mathcal{R}_0^{no\ mobility(2)}$, namely $\mathcal{R}_0^{one-way\ (2\to1)} = 3.9999 \approx 4$. The elasticity values of the parameters with respect to $\mathcal{R}_0^{one-way\ (2\to1)} = 3.9999$ are presented in the table and bar chart below.

Table 3. Elasticity Values of the Parameters with Respect to $\mathcal{R}_0^{one-way\ (2\to1)} = 3.9999$

Parameter	Parameter Unit	$\mathcal{R}_0^{one-way\ (2\to1)} = 3.9999$
Λ_1	individual / time	0.5983766785
Λ_2	individual / time	0.4016233212
β_1	1 / individual . time	**0.7955773330**
β_2	1 / individual . time	0.2044226664
q_1	non-dimensional	0.5983766789
q_2	non-dimensional	0.4016233211
P_2	non-dimensional	0.3944013094
α	1 / time	0.0001995689
δ	1 / time	−0.0645914973
γ	1 / time	**−0.8382684526**
ξ	1 / time	−0.09688724602
μ	1 / time	**−1.000452373**

Scenario 2: $\mathcal{R}_0^{no\ mobility(1)} > 1 > \mathcal{R}_0^{no\ mobility(2)}$

In this scenario, the parameter values are substituted into the elasticity equations for each parameter with respect to $\mathcal{R}_0^{one-way\ (2\to1)}$ such that the condition $\mathcal{R}_0^{no\ mobility(1)} > \mathcal{R}_0^{no\ mobility(2)} > 1$ is satisfied. The results obtained from this scenario are $\mathcal{R}_0^{no\ mobility(1)} = 1.5683$ and $\mathcal{R}_0^{no\ mobility(2)} = 0.4214$. Under this condition, the resulting value of $\mathcal{R}_0^{one-way\ (2\to1)}$ becomes higher than both, $\mathcal{R}_0^{no\ mobility(1)}$and $\mathcal{R}_0^{no\ mobility(2)}$, namely $\mathcal{R}_0^{one-way\ (2\to1)} = 2.0968$. The elasticity values of the parameters with respect to $\mathcal{R}_0^{one-way\ (2\to1)} = 2.0968$ are presented in the table and bar chart below.

Table 4. Elasticity Values of the Parameters with Respect to $\mathcal{R}_0^{one-way\ (2\to1)} = 2.0968$

Parameter	Parameter Unit	$\mathcal{R}_0^{one-way\ (2\to1)} = 2.0968$
Λ_1	individual / time	$\mathbf{0.7601891794}$
Λ_2	individual / time	0.2398108211
β_1	1 / individual . time	$\mathbf{0.9517983803}$
β_2	1 / individual . time	0.0482016202
q_1	non-dimensional	$\mathbf{0.7601891795}$
q_2	non-dimensional	0.2398108210
P_2	non-dimensional	0.3832184014
α	1 / time	0.0001995689
δ	1 / time	-0.06459149735
γ	1 / time	$\mathbf{-0.8382684526}$
ξ	1 / time	-0.0968872460
μ	1 / time	$\mathbf{-1.000452373}$

Scenario 3: $\mathcal{R}_0^{no\ mobility(2)} > 1 > \mathcal{R}_0^{no\ mobility(1)}$

In this scenario, the parameter values are substituted into the elasticity equations for each parameter with respect to $\mathcal{R}_0^{one-way\ (2\to1)}$ such that the condition $\mathcal{R}_0^{no\ mobility(1)} > \mathcal{R}_0^{no\ mobility(2)} > 1$ is satisfied. The results obtained from this scenario are $\mathcal{R}_0^{no\ mobility(1)} = 0.4214$ and $\mathcal{R}_0^{no\ mobility(2)} = 1.5683$. Under this condition, the resulting value of $\mathcal{R}_0^{one-way\ (2\to1)}$ becomes higher than both, $\mathcal{R}_0^{no\ mobility(1)}$and $\mathcal{R}_0^{no\ mobility(2)}$, namely $\mathcal{R}_0^{one-way\ (2\to1)} = 2.0968$. The elasticity values of the parameters with respect to $\mathcal{R}_0^{one-way\ (2\to1)} = 1.6216$ are presented in the table and bar chart below.

Table 5. Elasticity Values of the Parameters with Respect to $\mathcal{R}_0^{one-way\,(2\to1)} = 1.6216$

Parameter	Parameter Unit	$\boldsymbol{\mathcal{R}_0^{one-way\,(2\to1)} = 1.6216}$
Λ_1	individual / time	0.04250964160
Λ_2	individual / time	$\mathbf{0.9574903580}$
β_1	1 / individual . time	0.07397085038
β_2	1 / individual . time	$\mathbf{0.9260291494}$
q_1	non-dimensional	0.04250964153
q_2	non-dimensional	$\mathbf{0.9574903584}$
P_2	non-dimensional	0.06292241772
α	1 / time	0.00019956848
δ	1 / time	-0.06459149735
γ	1 / time	$\mathbf{-0.8382684526}$
ξ	1 / time	-0.09688724602
μ	1 / time	$\mathbf{-1.000452373}$

Across the three scenarios above, it can be observed that the parameters Λ_1, Λ_2, β_1, β_2, q_1, q_2, P_2, and α exert a positive influence on $\mathcal{R}_0^{one-way\,(2\to1)}$. Thus, increasing the values of these parameters will result in an increase in $\mathcal{R}_0^{one-way\,(2\to1)}$. However, it can also be noted that the parameter α has almost no effect on $\mathcal{R}_0^{one-way\,(2\to1)}$. In contrast, the parameters δ, γ, ξ, and μ have a negative influence on $\mathcal{R}_0^{one-way\,(2\to1)}$. Therefore, increasing these parameter values will lead to a decrease in $\mathcal{R}_0^{one-way\,(2\to1)}$. Moreover, the greater the absolute value of a parameter's elasticity, the greater its impact on $\mathcal{R}_0^{one-way\,(2\to1)}$.

The Autonomous Simulation of $\mathcal{R}_0$ for the One-Way Mobility Model

In this section, simulations are conducted to examine the effect of P_2 on the infected populations in each city $(E_1, E_2, A_1, A_2, I_1, I_2)$. In addition, the reproduction numbers in each city also play an important role in the simulations of this model. Therefore, several scenarios are considered based on the reproduction numbers in the two cities, namely $\mathcal{R}_0^{no\ mobility(1)}$ and $\mathcal{R}_0^{no\ mobility(2)}$. The following presents the autonomous simulation results for this model.

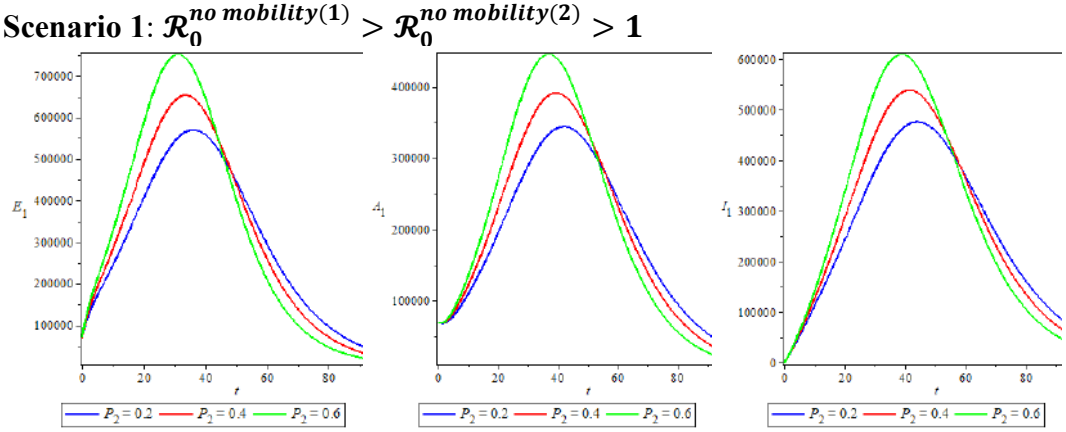

Figure 4. Effect of P_2 on the Infected Population in City 1 for Scenario 1 in the One-Way Mobility Model

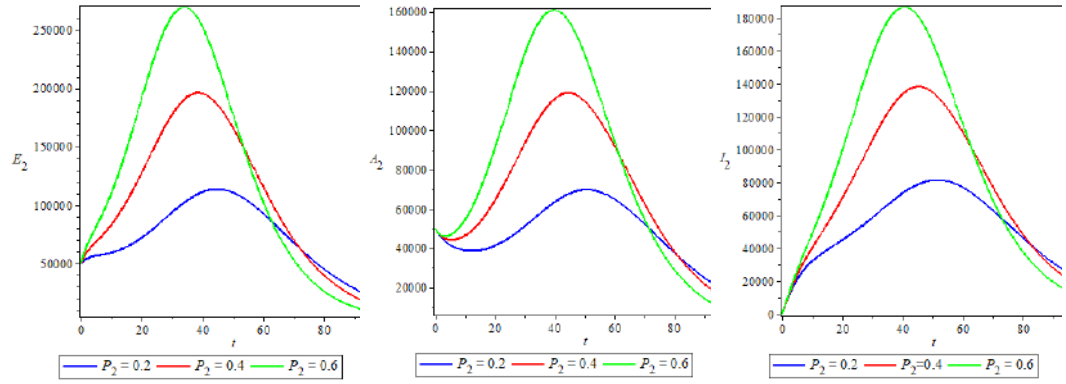

Figure 5. Effect of P_2 on the Infected Population in City 2 for Scenario 1 in the One-Way Mobility Model

Figure 4 and Figure 5 illustrate the autonomous simulation results showing the effect of P_2 on the infected populations in both cities under Scenario 1. The simulation results consistently show that increasing P_2 leads to higher peaks of exposed, asymptomatic, and symptomatic infected individuals in both cities. In City 1, which already has a higher transmission potential, the arrival of highly mobile individuals from City 2 intensifies disease spread, resulting in noticeably larger infection curves as P_2increases. This reflects the amplifying effect of one-way mobility on a city with stronger endemicity. Similarly, although movement occurs from City 2 to City 1, City 2 also experiences an increase in infection levels when P_2 is larger. This occurs because higher mobility implies higher social activity and contact rates within City 2 before individuals travel, thereby increasing local transmission.

Scenario 2: $\mathcal{R}_0^{no\ mobility(1)} > 1 > \mathcal{R}_0^{no\ mobility(2)}$

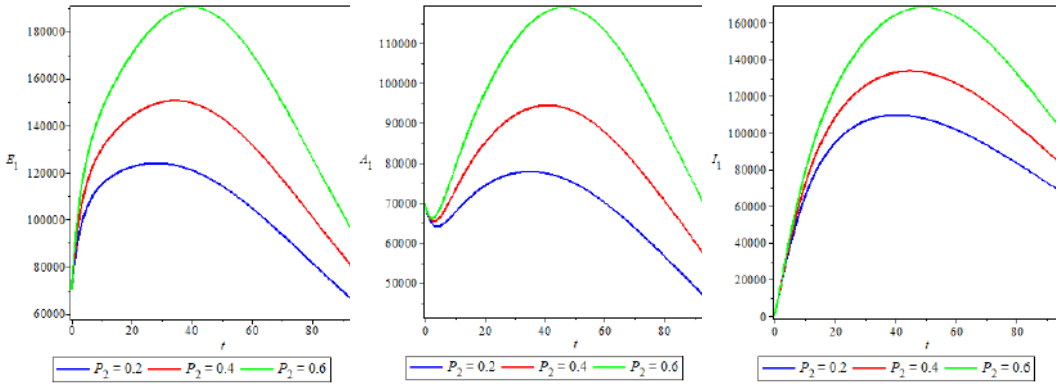

Figure 6. Effect of P_2 on the Infected Population in City 1 for Scenario 2 in the One-Way Mobility Model

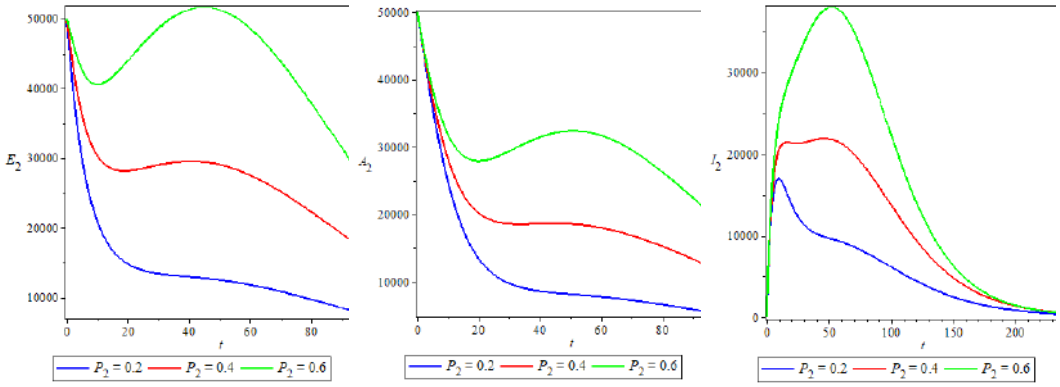

Figure 7. Effect of P_2 on the Infected Population in City 2 for Scenario 2 in the One-Way Mobility Model

Figure 6 and Figure 7 present the autonomous simulation results showing the effect of P_2 on the infected population in both cities under Scenario 2. In this scenario, only City 1 exhibits endemic behavior, while City 2 is theoretically subcritical in the absence of mobility. The simulation results show that increasing P_2 consistently raises the peak and overall magnitude of infected individuals in City 1. This occurs because the arrival of highly mobile susceptible individuals from City 2 amplifies transmission within City 1, which already has a reproduction number above unity. As P_2 increases, the curves in City 1 (Figure 9) become higher, indicating that one-way mobility strengthens the epidemic intensity in the higher-risk city. Although City 2 has $\mathcal{R}_0^{no\ mobility(2)} < 1$, Figure 10 shows that infection levels in City 2 also increase when P_2 becomes larger. This is due to the fact that a higher proportion of highly mobile individuals leads to greater social interaction within City 2 before they move to City 1, thereby increasing transmission locally despite the city being subcritical in isolation. The trajectories in City 2 become noticeably higher for larger P_2, especially in the early outbreak period, reflecting the role of mobility-driven contact patterns.

Scenario 3: $\mathcal{R}_0^{no\ mobility(2)} > 1 > \mathcal{R}_0^{no\ mobility(1)}$

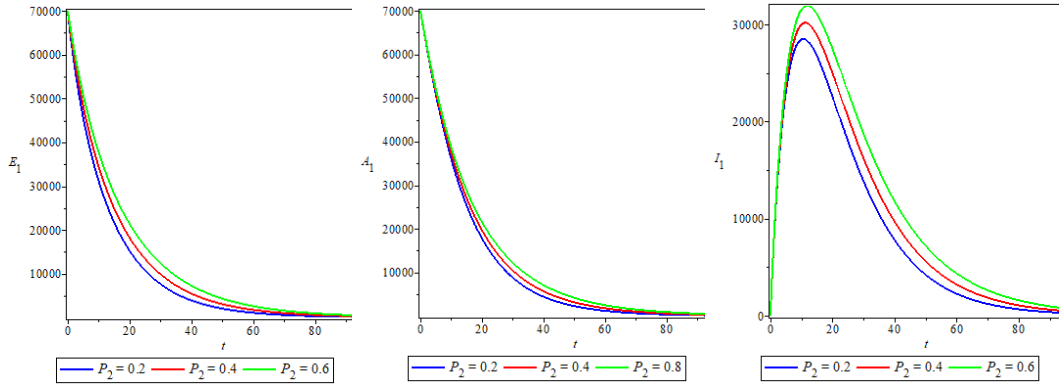

Figure 8. Effect of P_2 on the Infected Population in City 1 for Scenario 3 in the One-Way Mobility Model

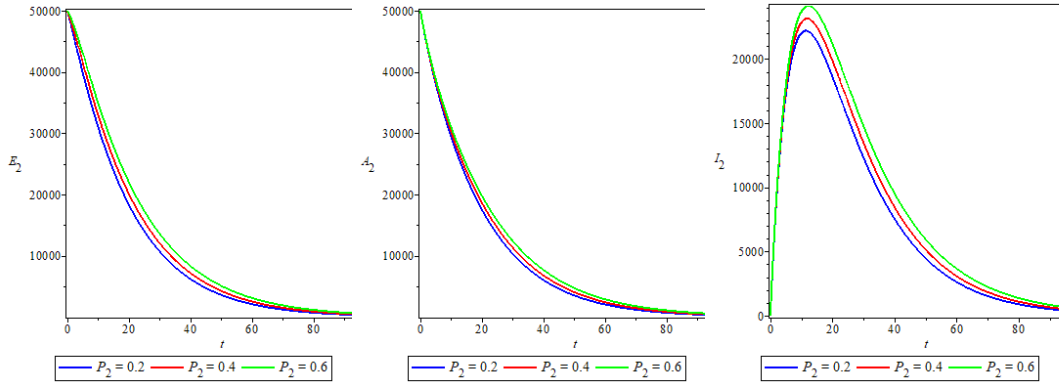

Figure 9. Effect of P_2 on the Infected Population in City 2 for Scenario 3 in the One-Way Mobility Model

Figures 8 and Figure 9 present the autonomous simulation results illustrating the effect of P_2 on the infected populations in both cities under Scenario 3. In this scenario, only City 2 is endemic, while City 1 is subcritical in the absence of mobility. The simulation results show that increasing P_2 leads to higher infection curves in City 1, particularly for the symptomatic class I_1. This indicates that one-way mobility from City 2 introduces a substantial number of imported cases into City 1, elevating infection levels in a city that would otherwise remain stable without mobility. The arrival of highly mobile individuals from an endemic region (City 2) effectively drives transmission in City 1, demonstrating the strong influence of mobility on disease spread across regions with differing transmission potentials. In City 2, shown in Figure 12, infection levels also increase with larger values of P_2, even though the city is already endemic. The rise occurs because higher mobility corresponds to greater social contact within City 2 prior to movement, thereby intensifying local transmission before individuals travel to City 1. Although the increase in City 2 is not as pronounced as in City 1, the upward

shift in all infection curves demonstrates that mobility amplifies disease burden in both the source and destination cities.

Before turning to the policy implications, it is worth clarifying how these time-dependent simulations relate to the equilibrium analysis. Because the model is autonomous, each trajectory approaches the steady state selected by the basic reproduction number: when the coupled reproduction number exceeds unity the infected compartments settle at a positive plateau consistent with the existence of an endemic state, whereas when it lies below unity they decay to zero, recovering the disease-free equilibrium whose local asymptotic stability was established in Theorem 2. The three scenarios above all correspond to a coupled reproduction number greater than unity; nevertheless, the subcritical case is not absent from the analysis, since in Scenario 2 the source city and in Scenario 3 the destination city are individually subcritical in isolation, so that sub- and supercritical cities already coexist within a single coupled system. To represent the fully subcritical regime as well, Figure 10 reports an additional simulation in which the mobility-related parameters are reduced so that the coupled reproduction number falls below unity; there, all infected compartments in both cities converge to zero, numerically confirming the stability result of Theorem 2 and complementing the supercritical scenarios.

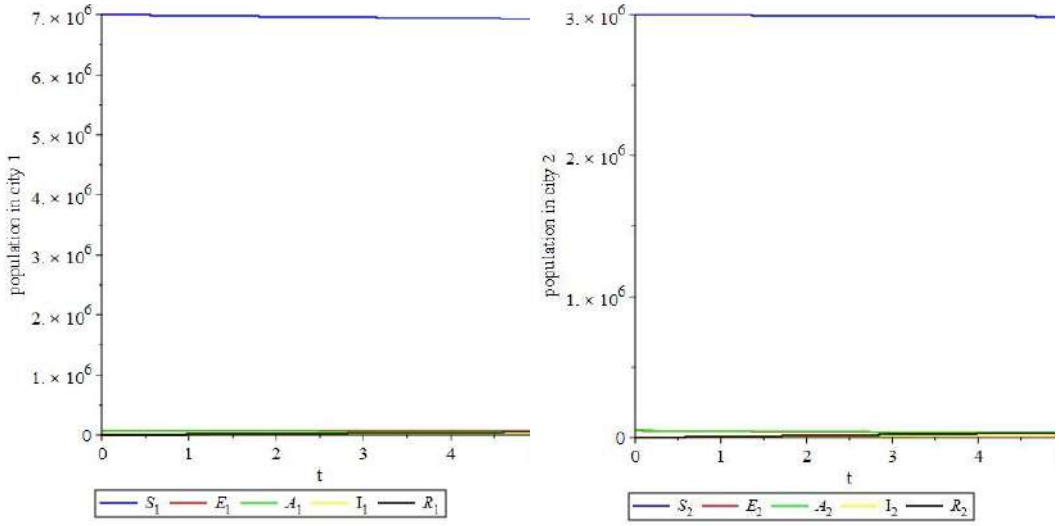

(a) (b)

Figure 10. Convergence to the disease-free equilibrium under a subcritical configuration of the one-way mobility model. (a) Population in city 1, and (b) Population in city 2.

These results carry distinct policy implications depending on the epidemiological configuration of the two cities. In Scenario 1, where both cities are already supercritical, mobility compounds two simultaneous outbreaks, so the priority is to reduce the proportion of highly mobile individuals and to enforce contact-reducing measures such as social distancing in the higher-transmission city. In Scenario 2, where the destination city is endemic but the source city is subcritical

in isolation, the dominant risk is that mobility raises contact rates within the source city itself; targeted measures within the source city, rather than only at the destination, are therefore most effective. In Scenario 3, where the source city is endemic and the destination city would otherwise remain stable, the destination is destabilized almost entirely by imported infections, so screening, testing, or movement restrictions applied to incoming highly mobile individuals yield the greatest benefit. Taken together, the scenarios show that effective control requires tailoring mobility-sensitive policies to which city carries the higher transmission potential, rather than applying uniform restrictions across regions.

CONCLUSION

This study has developed a COVID-19 transmission model that incorporates one-way human mobility, providing a more realistic representation of directed population flow between two interconnected regions. The mathematical analysis shows that introducing one way mobility substantially modifies the epidemic structure compared to the no-mobility setting, particularly through changes in the basic reproduction number $\mathcal{R}_0$. Using the Next Generation Matrix approach, the study successfully derived $\mathcal{R}_0$ and established stability conditions for the disease free equilibrium, demonstrating that mobility can shift a previously stable system into an unstable one. Elasticity analysis further reveals that mobility-related parameters exert a strong positive influence on $\mathcal{R}_0$, while recovery and mortality-related parameters give a negative contribution, thereby offering insight into which components most effectively control disease spread. These findings highlight the fundamental role of directed movement in shaping epidemic outcomes and emphasize the value of mathematically grounded approaches for understanding transmission dynamics. Simulation results conducted under three epidemiological scenarios consistently demonstrate that increasing the proportion of highly mobile individuals intensifies infection levels in both cities, regardless of which city is initially endemic. When mobility originates from a high-transmission city, the destination city can experience imported infections sufficient to elevate its epidemic trajectory. Meanwhile, the source city also experiences increased infections due to heightened contact rates before individuals depart, illustrating how one-way mobility amplifies disease burden at both ends of the mobility pathway. The simulations confirm that even limited unidirectional movement can significantly alter epidemic trajectories, and thus mobility-sensitive interventions such as movement restrictions, targeted screening, or social distancing policies become essential for controlling spread. Overall, the model developed in this study advances theoretical understanding of spatial disease transmission and offers practical insights for designing public health policies that account for asymmetric population movement.

The main contributions of this study can be summarized as follows. First, it extends the no-mobility two-city framework of Balya et al. (2025) to incorporate

strictly unidirectional movement, yielding a closed-form expression for the coupled basic reproduction number through the Next Generation Matrix. Second, it establishes the local asymptotic stability of the disease-free equilibrium via the Van den Driessche–Watmough conditions and identifies, through elasticity analysis, the parameters that most strongly drive transmission under directed movement. Third, it demonstrates numerically that one-way mobility can raise infection levels even in a city that is subcritical in isolation, quantifying the destabilizing effect of asymmetric movement across three representative scenarios.

Several limitations should nonetheless be acknowledged. The analysis focuses on the existence and stability of the disease-free equilibrium; a full characterization of the endemic equilibrium, the possibility of backward bifurcation, and an analysis of global stability are left for future work. In addition, the parameter values used here are representative rather than calibrated, so the model has not yet been validated against region-specific surveillance data. Future research will therefore pursue empirical calibration using local case data, an explicit treatment of the endemic equilibrium, and an extension of the framework to multiple regions and to time-varying or partially two-way mobility patterns.

ACKNOWLEDGEMENT

We would like to express our sincere gratitude to DPPM Kemdiktisaintek for providing research funding under the Beginner Lecturer Research (PDP) scheme for the 2025 fiscal year.

REFERENCES

Aldila, D., Ndii, M. Z., & Samiadji, B. M. (2020). Optimal Control on COVID-19 Eradication Program in Indonesia under the Effect of Community Awareness. *Mathematical Biosciences and Engineering*, *17*(6), 6355–6389. https://doi.org/10.3934/mbe.2020335

Aldila, D., Samiadji, B. M., Simorangkir, G. M., Khosnaw, S. H. A., & Shahzad, M. (2021). Impact of Early Detection and Vaccination Strategy in COVID-19 Eradication Program in Jakarta, Indonesia. *BMC Research Notes*, *14*(1). https://doi.org/10.1186/s13104-021-05540-9

Badr, H. S., Du, H., Marshall, M., Dong, E., Squire, M. M., & Gardner, L. M. (2021). Association Between Mobility Patterns and COVID-19 Transmission in the USA: a Mathematical Modelling Study. *The Lancet Infectious Diseases*, *20*(11), 1247–1254. https://doi.org/10.1016/S1473-3099(20)30553-3

Balya, M. A., Aldila, D., Yulida, Y., Rizqina, S., & Affandi, P. (2025). Analyzing COVID-19 Dynamics in Two Non-Interacting Regions through a Structured Compartmental Model. *Epsilon: Jurnal Matematika Murni Dan Terapan*, *19*, 54–71. http://ppjp.ulm.ac.id/journals/index.php/epsilon

Balya, M. A., Dewi, B. O., Lestari, F. I., Ratu, G., Rosuliyana, H., Windyhani, T., Fadhlia, Z. R., Samiadji, B. M., Aldila, D., Khoshnaw, S. H. A., & Shahzad, M. (2021). Investigating the Impact of Social Awareness and Rapid Test on a COVID-19 Transmission Model. *Communication in Biomathematical Sciences*, *4*(1), 46–64. https://doi.org/10.5614/cbms.2021.4.1.5

Boyce, W. E., & DiPrima, R. C. (2009). *Elementary Differential Equations and Boundary Value Problems* (ninth). John Wiley & Sons.

Braun, M. (1993). *Differential Equations and the Applications* (Fourth). Springer.

Chitnis, N., Hyman, J. M., & Cushing, J. M. (2008). Determining Important Parameters in the Spread of Malaria through the Sensitivity Analysis of a Mathematical Model. *Bulletin of Mathematical Biology*, *70*(5), 1272–1296. https://doi.org/10.1007/s11538-008-9299-0

Del Rio, C., & Malani, P. N. (2020). COVID-19 - New Insights on a Rapidly Changing Epidemic. In *JAMA - Journal of the American Medical Association* (Vol. 323, Number 14, pp. 1339–1340). American Medical Association. https://doi.org/10.1001/jama.2020.3072

Diekmann, O., Heesterbeek, J. A. P., & Roberts, M. G. (2010). The Construction of Next-Generation Matrices for Compartmental Epidemic Models. *Journal of the Royal Society Interface*, *7*(47), 873–885. https://doi.org/10.1098/rsif.2009.0386

Feng, Z., & Velasco-Herna´ndezherna´ndez, J. X. (1997). Competitive Exclusion in a Vector-Host Model for the Dengue Fever. *J. Math. Biol*, *35*, 523–544.

Flaxman, S., Mishra, S., Gandy, A., Unwin, H. J. T., Mellan, T. A., Coupland, H., Whittaker, C., Zhu, H., Berah, T., Eaton, J. W., Monod, M., Perez-Guzman, P. N., Schmit, N., Cilloni, L., Ainslie, K. E. C., Baguelin, M., Boonyasiri, A., Boyd, O., Cattarino, L., … Bhatt, S. (2021). Estimating the Effects of Non-Pharmaceutical Interventions on COVID-19 in Europe. *Nature*, *584*(7820), 257–261. https://doi.org/10.1038/s41586-020-2405-7

He, S., Peng, Y., & Sun, K. (2020). SEIR Modeling of the COVID-19 and Its Dynamics. *Nonlinear Dynamics*, *101*(3), 1667–1680. https://doi.org/10.1007/s11071-020-05743-y

Iyaniwura, S. A., Ringa, N., Adu, P. A., Mak, S., Janjua, N. Z., Irvine, M. A., et al. (2023). Understanding the Impact of Mobility on COVID-19 Spread: a Hybrid Gravity-Metapopulation Model of COVID-19. *PLOS Computational Biology*, *19*(5), e1011123. https://doi.org/10.1371/journal.pcbi.1011123

Jia, J. S., Lu, X., Yuan, Y., Xu, G., Jia, J., & Christakis, N. A. (2021). Population Flow Drives Spatio-Temporal Distribution of COVID-19 in China. *Nature*, *582*(7812), 389–394. https://doi.org/10.1038/s41586-020-2284-y

Lai, C. C., Shih, T. P., Ko, W. C., Tang, H. J., & Hsueh, P. R. (2021). Severe Acute Respiratory Syndrome Coronavirus 2 (SARS-CoV-2) and Coronavirus Disease-2019 (COVID-19): The Epidemic and the Challenges. In *International Journal of Antimicrobial Agents* (Vol. 55, Number 3). Elsevier B.V. https://doi.org/10.1016/j.ijantimicag.2020.105924

Lauer, S. A., Grantz, K. H., Bi, Q., Jones, F. K., Zheng, Q., Meredith, H. R., Azman, A. S., Reich, N. G., & Lessler, J. (2020). The Incubation Period of Coronavirus Disease 2019 (CoVID-19) from Publicly Reported Confirmed Cases: Estimation and Application. *Annals of Internal Medicine*, *172*(9), 577–582. https://doi.org/10.7326/M20-0504

Li, Q., Guan, X., Wu, P., Wang, X., Zhou, L., Tong, Y., Ren, R., Leung, K. S. M., Lau, E. H. Y., Wong, J. Y., Xing, X., Xiang, N., Wu, Y., Li, C., Chen, Q., Li, D., Liu, T., Zhao, J., Liu, M., … Feng, Z. (2020). Early Transmission Dynamics in Wuhan, China, of Novel Coronavirus–Infected Pneumonia. *New*

England Journal of Medicine, *382*(13), 1199–1207. https://doi.org/10.1056/nejmoa2001316

Lin, J., Wu, K., Yang, S., & Liu, Q. (2021). The Asymmetric Pattern of Population Mobility During the Spring Festival in the Yangtze River Delta Based on Complex Network Analysis: An Empirical Analysis of "Tencent Migration" Big Data. *ISPRS International Journal of Geo-Information*, *10*(9). https://doi.org/10.3390/ijgi10090582

Martcheva, M. (2015). *An Introduction to Mathematical Epidemiology* (Vol. 61). Springer. https://doi.org/10.1007/978-1-4899-7612-3

Pei, S., & Shaman, J. (2020). *Initial Simulation of SARS-CoV2 Spread and Intervention Effects in the Continental US*. https://doi.org/10.1101/2020.03.21.20040303

Van Den Driessche, P., & Watmough, J. (2002). Reproduction Numbers and Sub-Threshold Endemic Equilibria for Compartmental Models of Disease Transmission. *Mathematical Biosciences*, 29–48. www.elsevier.com/locate/mbs

Wiggins, S. (2003). *Introduction to Applied Nonlinear Dynamical Systems and Chaos* (Second). Springer-Verlag New York, Inc.

Yang, C., & Wang, J. (2020). A Mathematical Model for the Novel Coronavirus Epidemic in Wuhan, China. *Mathematical Biosciences and Engineering*, *17*(3), 2708–2724. https://doi.org/10.3934/mbe.2020148